Nuclear Envelope Disruption Involving Host Caspases Plays a Role in the Parvovirus Replication Cycle[▽]

Sarah Cohen, Alexandra K. Marr, Pierre Garcin, and Nelly Panté*

Department of Zoology, University of British Columbia, 6270 University Boulevard, Vancouver, British Columbia, Canada V6T 1Z4

Parvoviruses are small, nonenveloped, single-stranded DNA viruses which replicate in the nucleus of the host cell. We have previously found that early during infection the parvovirus minute virus of mice (MVM) causes small, transient disruptions of the nuclear envelope (NE). We have now investigated the mechanism used by MVM to disrupt the NE. Here we show that the viral phospholipase A2, the only known enzymatic domain on the parvovirus capsid, is not involved in causing NE disruption. Instead, the virus utilizes host cell caspases, which are proteases involved in causing NE breakdown during apoptosis, to facilitate these nuclear membrane disruptions. Studies with pharmacological inhibitors indicate that caspase-3 in particular is involved. A caspase-3 inhibitor prevents nuclear lamin cleavage and NE disruption in MVM-infected mouse fibroblast cells and reduces nuclear entry of MVM capsids and viral gene expression. Caspase-3 is, however, not activated above basal levels in MVM-infected cells, and other aspects of apoptosis are not triggered during early MVM infection. Instead, basally active caspase-3 is relocalized to the nuclei of infected cells. We propose that NE disruption involving caspases plays a role in (i) parvovirus entry into the nucleus and (ii) alteration of the compartmentalization of host proteins in a way that is favorable for the virus.

In order to replicate successfully, viruses must overcome various barriers in the cell. For viruses that replicate in the cell nucleus, the nuclear envelope (NE) is one such barrier. The NE consists of an inner nuclear membrane (INM) and an outer nuclear membrane (ONM). These membranes are supported by an underlying protein meshwork called the nuclear lamina, composed of the intermediate filament proteins nuclear lamins, which is associated with the nuclear face of the NE. Embedded in the NE are the nuclear pore complexes (NPCs), which are large protein complexes that mediate active transport of molecules up to 39 nm in diameter into and out of the nucleus (40). Because the sizes and structures of viruses vary enormously, viruses have developed surprisingly diverse strategies for delivering their genome and accessory proteins into the nuclei of infected cells (21, 26, 60, 61). Aside from some retroviruses, which are thought to enter the nucleus while the NE is disassembled during mitosis (19), most of these strategies involve partial disassembly of the virion and nuclear transport through the NPC using the cellular nuclear import machinery (i.e., nuclear localization signals, importins, GTP, and Ran) (55). The viral component entering the nucleus may be an intact capsid (e.g., hepatitis B virus capsid, which crosses the NPC intact [40, 42]), a naked viral genome (e.g., for herpes simplex virus type 1 which ejects its DNA from its NPC-docked capsid into the nucleus, leaving empty capsids at the NPC [51]), or a viral genome in association with viral proteins (e.g., influenza virus ribonucleoprotein complexes [11]).

In general, more is known about the nuclear entry of enveloped viruses than about that of nonenveloped viruses. Thus, we are using the small, nonenveloped parvovirus minute virus of mice (MVM) as a model to study nuclear entry of nonenveloped viruses. After entering a host cell by endocytosis, parvoviruses slowly escape from endocytic compartments to the cytoplasm (10, 25). Because the MVM capsid is only about 26 nm in diameter (10), it has been largely assumed that parvoviruses enter the nucleus intact through the NPC. However, we recently found that MVM causes small disruptions in the NE and alterations in the nuclear lamin immunostaining of infected fibroblast cells as early as 1 h postinfection (6). These disruptions coincide with the perinuclear location of the virus in the cell, suggesting that MVM enters the nucleus by a novel mechanism: disruption of the NE and entry through the resulting breaks. Consistent with this idea, capsids of the parvovirus adeno-associated virus 2 (AAV2) were previously shown to enter purified nuclei in an NPC-independent manner (24).

Our hypothesis is that MVM hijacks a cellular mechanism for nuclear envelope breakdown (NEBD). During mitotic NEBD, NPC proteins and nuclear lamins are phosphorylated, resulting in disassembly of both NPCs and the nuclear lamina (23). During apoptotic NEBD, NPC proteins and nuclear lamins are both phosphorylated and cleaved (15, 46). We have investigated the involvement of host enzymes used during apoptotic NEBD in MVM-induced NE disruption. We found that MVM utilized a relocalization of caspase-3 to facilitate transient disruptions of the NE, which resealed later in infection and did not coincide with complete apoptosis leading to double-stranded DNA breaks. Inhibition of caspase-3 during infection of cells with MVM resulted in a significant reduction in nuclear entry of MVM capsids and virus early gene expression, suggesting that NE disruption is important for the parvovirus replication cycle.

* Corresponding author. Mailing address: Department of Zoology, University of British Columbia, 6270 University Boulevard, Vancouver, BC, Canada V6T 1Z4. Phone: (604) 822-3369 Fax: (604) 822-2416 E-mail: pante@zoology.ubc.ca.

MATERIALS AND METHODS

Cells and virus. Adherent LA9 mouse fibroblast cells (30) and HeLa cells stably expressing a fusion of green fluorescent protein to lamina-associated polypeptide 2β (GFP-LAP2β) (courtesy of U. Kutay, ETH Zurich) were maintained at 5% CO_2 and 37°C in complete Dulbecco's modified Eagle's medium (DMEM) supplemented with 10% fetal bovine serum (FBS) and penicillin-streptomycin. Wild-type MVM was purified as previously described (2). MVM with an H42R mutation was a gift from P. Tattersall (Yale University School of Medicine).

***Xenopus* oocyte microinjection and electron microscopy.** *Xenopus* oocytes were mock injected with phosphate-buffered saline (PBS) or injected with 50 nl of MVM (1×10^8 PFU/ml, approximately equal to 6×10^{10} genomes/ml) or H42R-MVM (6×10^{10} genomes/ml). For the phospholipase A2 (PLA2) inhibition experiment, MVM was incubated with 10 μM manoalide (Alexis Biochemicals) for 1 h at room temperature with agitation prior to microinjection. Where indicated, a 50 mM concentration of the caspase inhibitor benzyloxycarbonyl-Val-Ala-Asp-fluoromethyl ketone (zVAD-fmk), zDEVD-fmk, or zVEID-fmk (Tocris Biosciences) was included in the MVM solution to be injected, resulting in an intracellular inhibitor concentration of approximately 200 μM. Oocytes were then incubated at room temperature for 2 h, followed by fixation and preparation for thin-section electron microscopy (EM) as previously described (2, 5, 39). Quantification of the proportion of ONM damaged was performed using ImageJ software (National Institutes of Health).

Enzymatic activity assays. The PLA2 activity of MVM particles was assayed using a PLA2 activity kit (Cayman Chemical) according to the manufacturer's instructions. For the PLA2 inhibition assay, 5 μg of MVM particles was incubated with 10 μM manoalide (Alexis Biochemicals) for 1 h at room temperature with agitation before PLA2 activity was measured. The caspase-3 activity of lysates from cells that were mock infected, infected with MVM for 2 h as described below, or treated with 1 μM staurosporine (STS) (Alexis Biochemicals) for 6 h was measured using a colorimetric caspase-3 cellular assay kit (Biomol) according to the manufacturer's instructions.

Semipermeabilized cell assay for NE disruption. Evenly spread GFP-LAP2β HeLa cells grown in μ-slide eight-well dishes (Ibidi; ibiTreat) were washed in permeabilization buffer (PB) (20 mM HEPES KOH [pH 7.4], 110 mM potassium acetate [KOAc], 5 mM MgOAc, 0.5 mM EGTA, and 250 mM sucrose), permeabilized in PB containing 15 μg/ml digitonin for 3 min, and then washed three times in PB for 2 min. Permeabilized cells were then incubated or mock incubated with MVM at a multiplicity of infection (MOI) of 4 PFU/cell in transport buffer (TB) (20 mM HEPES KOH [pH 7.3], 110 mM KOAc, 5 mM NaOAc, 1 mM EGTA, and 2 mM dithiothreitol [DTT]) containing 155-kDa tetramethyl rhodamine isocyanate (TRITC)-labeled dextran (250 μg/ml) (Sigma-Aldrich) and visualized immediately on an Olympus Fluoview FV1000 laser scanning microscope at 37°C. Where indicated, the caspase inhibitor zVAD-fmk (200 μM), zDEVD-fmk (50 μM), or zVEID-fmk (50 μM) (Tocris Biosciences) was included in the last washing step and the incubation/visualization step. Quantification of nuclear over extracellular fluorescence was performed by measuring the mean fluorescence intensity of a defined area (10 pixels by 10 pixels) in the nucleus and dividing by the mean intensity of an equal area outside the cell, using ImageJ software (National Institutes of Health).

Transfection and infection. For transient expression of tandem GFP (5GFP), LA9 cells were grown in monolayers on poly-L-lysine-coated coverslips and transfected using Lipofectamine 2000 (Invitrogen), according to the manufacturer's instructions, at 48 h prior to infection with MVM. For infection, LA9 cells were grown in monolayers on poly-L-lysine-coated coverslips or in 10-cm dishes and then mock infected or infected with MVM at an MOI of 4 PFU/cell in DMEM supplemented with 1% FBS. Cells were incubated for 1 h at 4°C to allow the virus to bind at the cell surface. The medium was then replaced, and cells were incubated at 37°C for 2, 15, or 21 h. Where indicated, the caspase inhibitor zVAD-fmk, zDEVD-fmk, or zVEID-fmk (Tocris Biosciences) was included in the medium for 1 h prior to infection and during the infection steps.

Immunofluorescence (IF) microscopy. For lamin A/C immunostaining, cells were first permeabilized (0.2% Triton X-100, 30 s) and then fixed (3% paraformaldehyde, 3 min), blocked (2% bovine serum albumin [BSA], 20 min), and labeled with primary antibodies for intact MVM capsids (1:100, monoclonal; provided by P. Tattersall) and lamin A/C (1:200; Santa Cruz Biotechnology, H-110). For caspase-3 immunostaining, cells were fixed (3% paraformaldehyde, 10 min) and then permeabilized (ice-cold methanol, 10 min, −20°C), blocked (0.3% Triton X-100, 5% normal goat serum, 1 h), and labeled with primary antibodies for MVM (1:100, monoclonal; provided by P. Tattersall) and cleaved caspase-3 (1:25; Cell Signaling Technology, Asp-175). For MVM immunostaining of cells transfected with 5GFP and nonstructural protein 1 (NS1) immuno-

staining, cells were fixed (3% paraformaldehyde, 10 min) and then permeabilized (0.2% Triton X-100, 5 min), blocked (1% BSA, 1 h), and labeled with a primary antibody for MVM (1:100, monoclonal; provided by P. Tattersall) or NS1 (1:300, monoclonal; provided by P. Tattersall). All primary antibodies were followed by appropriate fluorescently labeled secondary antibodies (Invitrogen). Coverslips were mounted with Prolong Gold Antifade with 4′,6′-diamidino-2-phenylindole (DAPI) (Invitrogen) and visualized using a Zeiss Axioplan 2 fluorescence microscope (lamin A/C and NS1 experiments) or an Olympus Fluoview FV1000 laser scanning microscope (caspase-3 and 5GFP experiments). Quantification of the cells expressing NS1 was performed by threshold analysis using ImageJ software (National Institutes of Health).

Western blotting. LA9 cells were grown and infected as described above and then lysed in PBS containing 0.5% NP-40 and a protease inhibitor mixture (Roche Applied Science) on ice for 30 min. Lysates were cleared by centrifugation at $16,000 \times g$ for 5 min at 4°C. The supernatants were mixed with SDS-PAGE sample buffer, and aliquots with equal amounts of protein were loaded on an SDS-polyacrylamide gel. Proteins were transferred to nitrocellulose membranes, and proteins present in the lysates were detected by Western blotting using antibodies for lamin A/C (1:200; Santa Cruz Biotechnology, H-110) or lamin B (1:200; Santa Cruz Biotechnology, C-20). Image Pro Plus software (Media Cybernetics) was used to quantify the intensity of the smallest lamin B cleavage product. A minimum threshold of detection was determined in order not to include background. The intensity of the band was then determined by measuring the signal within a square area, the size of which was kept the same for measuring each band.

Immunogold electron microscopy. Monolayers of LA9 cells were grown in 10-cm dishes and infected with MVM as described above. Cells were fixed with 4% paraformaldehyde for 1 h and harvested by scraping. The resulting cell pellets were embedded for immunogold EM as previously described (2). For immunogold labeling, grids containing EM sections were blocked (2% BSA, three times for 10 min each), labeled with primary antibody for intact MVM capsids (1:5, monoclonal; provided by P. Tattersall) and secondary antibody (1:50, goat anti-mouse conjugated to 10-nm gold; Ted Pella). Finally, grids were stained with 2% uranyl acetate and 2% lead citrate and then visualized using a Hitachi H7600 transmission EM (TEM).

RESULTS

Viral PLA2 activity is not required for MVM-induced NE disruption. It has been shown that the MVM capsid has PLA2 activity, which can be abrogated by an H42R point mutation within the PLA2 active site of the capsid protein VP1 (16). Since the viral PLA2 is the only known enzymatic domain on the MVM capsid, we tested whether PLA2 activity was necessary for MVM-induced NE disruption using microinjection in *Xenopus* oocytes followed by EM. It was necessary to use microinjection rather than infection because under conditions of PLA2 inhibition, MVM capsids are unable to escape from endosomes (16), preventing access to the NE. Microinjection of *Xenopus* oocytes is a very good system for studying effects on the NE, because the oocytes yield nuclear membranes and NPCs that are very well preserved for EM. Therefore, oocytes were injected with MVM that has the H42R mutation (H24R-MVM). As controls, oocytes were mock injected with buffer or injected with wild-type MVM. Less MVM was injected than in previously published experiments (7) in order to more closely approximate physiological conditions. While the mock-injected oocytes yielded intact nuclear membranes, the MVM-injected oocytes showed frequent ONM disruptions of about 50 to 100 nm at 2 h postinjection (Fig. 1A). The H42R-MVM-injected oocytes also displayed frequent NE disruptions, suggesting that the viral PLA2 activity is not necessary for MVM-induced NE disruption. To confirm these results, we performed experiments inhibiting the PLA2 activity of wild-type MVM with the drug manoalide. First, to determine that the manoalide treatment was effectively inhibiting the viral PLA2, the PLA2 ac-
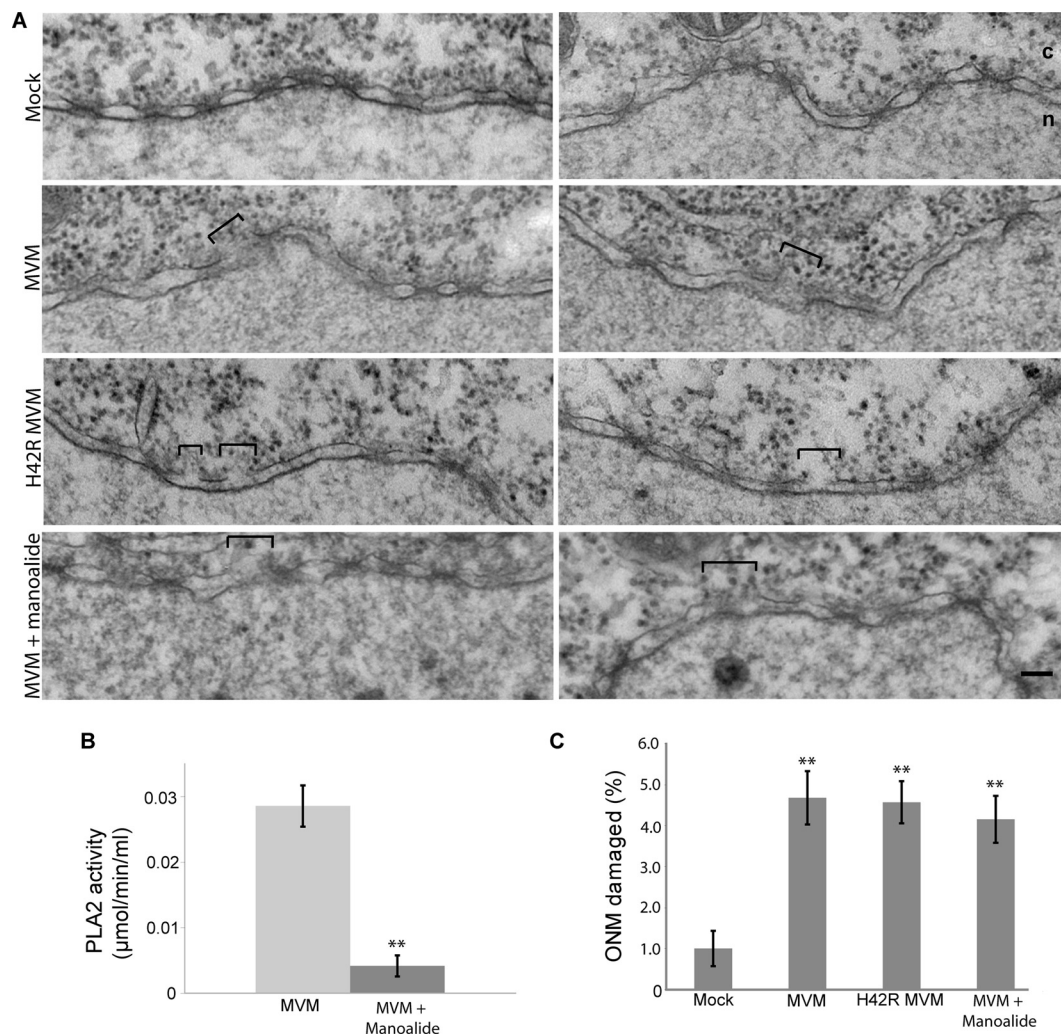
FIG. 1. MVM-induced NE disruption does not involve viral PLA2 activity. (A) Views of NE cross sections with adjacent cytoplasm (c) and nucleus (n) from *Xenopus* oocytes that have been mock injected or injected with wild-type MVM, H42R-MVM, or manoalide-treated MVM. Two representative NE views are shown for each condition. After injection, oocytes were incubated for 2 h at room temperature and processed for embedding and thin-section EM. Brackets indicate disruptions in the NE caused by MVM. Scale bar, 100 nm. (B) Colorimetric assay for PLA2 activity of untreated and manoalide-treated MVM. Values are means and standard deviations measured from three independent experiments. **, $P < 0.01$ compared to MVM (unpaired Student t test). (C) Proportion of NE damage, calculated as the length of the ONM breaks divided by the total length of the ONM from electron micrographs of experiments performed as indicated for panel A. Shown are the mean values and standard errors measured for 30 micrographs obtained from three different oocytes examined for each condition. **, $P < 0.01$ compared to mock infection (unpaired Student t test).

tivities of untreated MVM capsids and MVM capsids treated with manoalide were tested using an enzymatic activity assay (Fig. 1B). The PLA2 activity of manoalide-treated MVM capsids was reduced approximately 7-fold compared to that of untreated capsids. Next, MVM treated with manoalide was injected into *Xenopus* oocytes. Consistent with the results from H42R-MVM, the manoalide-treated MVM also disrupted the NE of the injected oocytes (Fig. 1A). Quantification revealed that injection of H42R MVM or manoalide-treated MVM caused just as much ONM damage as injection of untreated wild-type MVM (Fig. 1C). These results suggest that the viral PLA2 is not responsible for MVM-induced NE disruption.

Semipermeabilized cells can be used to assay for inhibitors of MVM-induced NE disruption. Since the viral PLA2 was

found not to be involved in MVM-induced NE disruption, we hypothesized that MVM might be hijacking a cellular program for NEBD normally used during mitosis or apoptosis. To test the involvement of various host enzymes in MVM-induced NE disruption, we modified a previously established *in vitro* nuclear disassembly system used to study mitotic NEBD (36). In this assay, HeLa cells expressing GFP-LAP2β as an NE marker were semipermeabilized with digitonin, which permeabilizes the plasma membrane but not the NE. Semipermeabilized cells were then incubated with MVM at an MOI of 4, and MVM-induced NE permeabilization was visualized by monitoring the nuclear influx of a large (155-kDa) TRITC-labeled dextran (Fig. 2A). In the absence of MVM (mock-incubated cells), the NE remained impermeable to the dextran over a 30-min time period, and the nuclei appeared black (Fig. 2A,
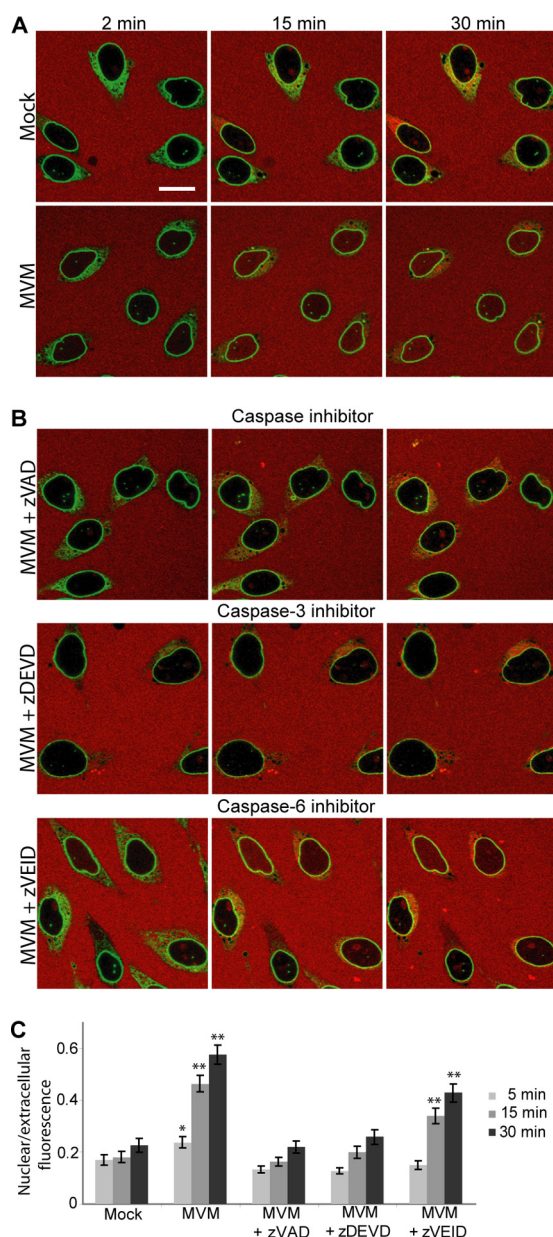
FIG. 2. MVM-induced NE disruption in semipermeabilized cells depends on caspases. (A) HeLa cells stably expressing GFP-LAP2β (green) were permeabilized with digitonin and then mock incubated or incubated with MVM (MOI of 4) in the presence of 155-kDa TRITC-dextran (red). In the absence of MVM, the NE remained impermeable to the dextran and the nuclei appear black. However, in the presence of MVM, the NE was disrupted and the TRITC-dextran entered the nucleus. (B) GFP-LAP2β HeLa cells were assayed for MVM-induced NE disruption as indicated for panel A in the presence of MVM (MOI of 4) and the pancaspase inhibitor zVAD-fmk (200 μM), the caspase-3 inhibitor zDEVD-fmk (50 μM), or the caspase-6 inhibitor Z-VEID-fmk (50 μM). While zVAD-fmk and zDEVD-fmk completely inhibited dextran leakage into the nucleus, zVEID-fmk did not. Scale bar, 5 μm. (C) Mean ratio of nuclear to extracellular fluorescence intensity and standard error for 40 cells per condition, from three independent experiments performed as described above. *, $P < 0.05$; **, $P < 0.01$ (compared to mock infection at the same time point by unpaired Student t test).

Mock) with some small green dots that are the results of normal invaginations of the NE (18). However, in the presence of MVM the TRITC-dextran entered the nucleus (Fig. 2A, MVM). Thus, similar to the case for MVM-infected cells (6), MVM disrupts the NE in the semipermeabilized cell system.

MVM-induced NE disruption involves caspases. We next performed the semipermeabilized cell assay for MVM-induced NE permeabilization in the presence of an array of inhibitors of host cell kinases and proteases implicated in mitotic or apoptotic NEBD (data not shown). Of the inhibitors tested, addition of the pancaspase inhibitor zVAD-fmk, a cell-permeative broad-spectrum inhibitor of caspases (14), most efficiently inhibited MVM-induced NE permeabilization. Caspases are proteases known to be responsible for cleaving NE proteins such as nucleoporins and nuclear lamins during apoptotic NEBD (15, 46). As illustrated in Fig. 2B and C, like the nuclei of mock-incubated semipermeabilized cells, the nuclei of semipermeabilized cells incubated with MVM in the presence of 200 μM zVAD-fmk remained impermeable to the dextran over a 30-min time period. A dose-dependent decrease of the NE permeability of cells incubated with MVM and zVAD-fmk was observed, with the most efficient inhibitory effect at 200 μM zVAD-fmk (data not shown).

We subsequently attempted to narrow down which caspase might be involved. Nuclear lamins are cleaved by caspase-3 and caspase-6 during apoptosis (38, 50, 54). Thus, we decided to test the caspase-3 inhibitor zDEVD-fmk and the caspase-6 inhibitor zVEID-fmk in our semipermeabilized cell assay (14, 56). As illustrated in Fig. 2B and C, while the caspase-3 inhibitor zDEVD-fmk (50 μM) completely inhibited the influx of fluorescent dextran into the nucleus in the presence of MVM, the caspase-6 inhibitor zVEID-fmk (50 μM) did not. The lower concentration was used to increase inhibitor specificity. Therefore, it seems that caspase-3 is especially important for MVM-induced NE permeabilization.

We wanted to confirm that the increase in NE permeability that we observed in our semipermeabilized cell assay correlated with the NE disruptions that we previously observed by EM and was not due to some other effect of the virus. Therefore, we mock injected or injected MVM into *Xenopus* oocytes in the absence or presence of the caspase inhibitors mentioned above. As in previous experiments, the mock-injected oocytes yielded intact nuclear membranes, while the MVM-injected oocytes showed frequent ONM disruptions at 2 h postinjection (Fig. 3A). Coinjection of MVM with either the pancaspase inhibitor zVAD-fmk or the caspase-3 inhibitor zDEVD-fmk completely prevented these NE disruptions, while coinjection of MVM with the caspase-6 inhibitor zVEID-fmk did not (Fig. 3A and B).

Clearly, as in the semipermeabilized cell assay, the pancaspase and caspase-3 inhibitors were more effective at inhibiting MVM-induced NE disruption than was the caspase-6 inhibitor. In addition we conclude that the changes in NE permeability that we observed in the semipermeabilized cell assay correlate with the nuclear membrane disruptions visualized by EM, since both are observed under the same conditions.

Caspases are involved in MVM-induced NE disruption and lamin cleavage in infected cells. We have previously demon-
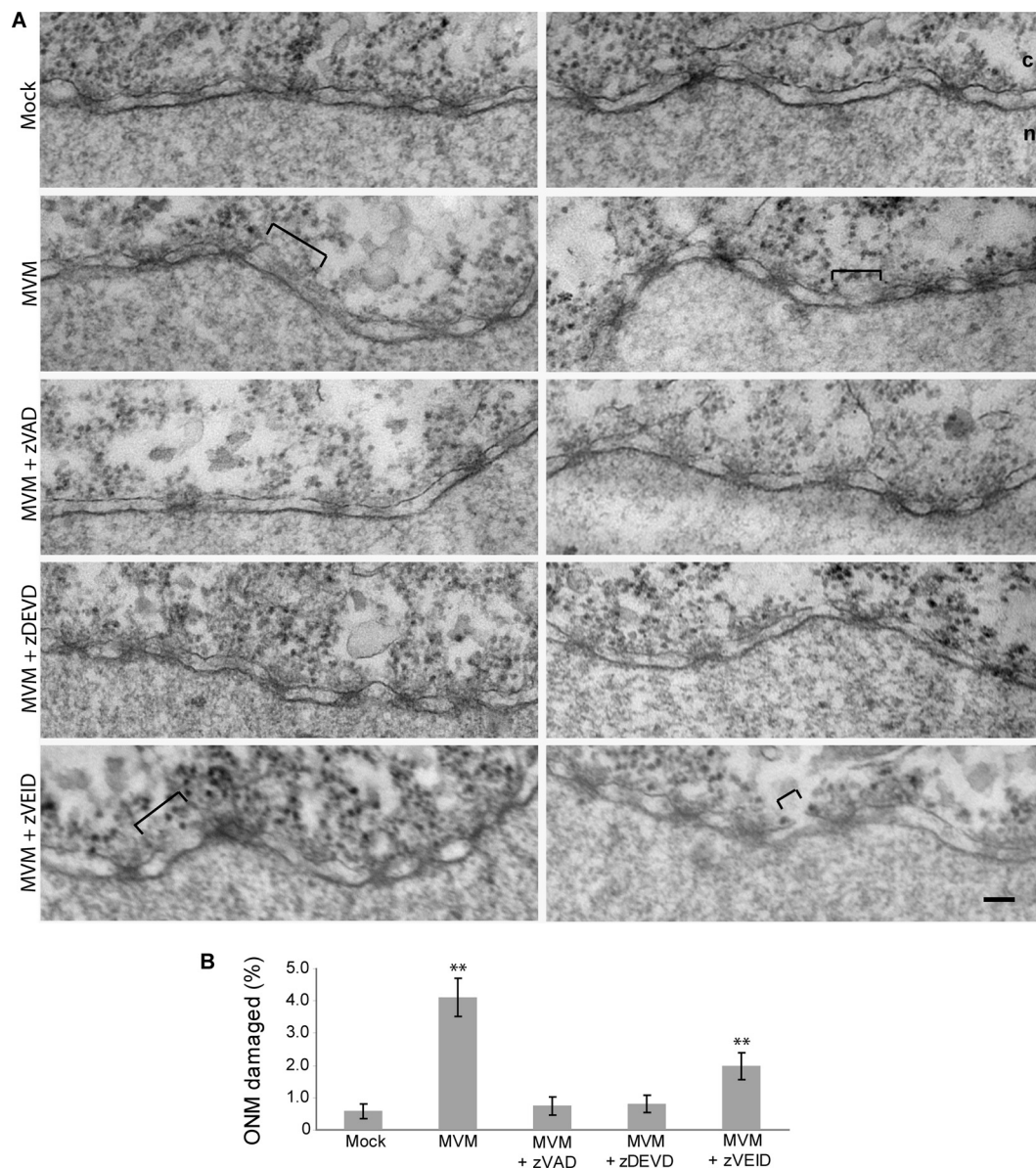
FIG. 3. Caspase inhibitors prevent NE disruption in MVM-injected *Xenopus* oocytes. (A) Views of NE cross sections with adjacent cytoplasm (c) and nucleus (n) from *Xenopus* oocytes that have been mock injected, injected with MVM, or coinjected with MVM and one of three caspase inhibitors: the pancaspase inhibitor zVAD-fmk, the caspase-3 inhibitor zDEVD-fmk, or the caspase-6 inhibitor zVEID-fmk. Two representative NE views are shown for each condition. After injection, oocytes were incubated for 2 h at room temperature and processed for embedding and thin-section EM. Brackets indicate disruptions in the NE caused by MVM. While zVAD-fmk and zDEVD-fmk completely inhibited disruption of the NE, zVEID-fmk did not. Scale bar, 100 nm. (B) Proportion of NE damage, calculated as the length of the ONM breaks divided by the total length of the ONM from electron micrographs of experiments performed as indicated above. Shown are the mean values and standard errors measured for 30 micrographs obtained from three different oocytes examined for each condition. ∗∗, $P < 0.01$ compared to mock infection (unpaired Student t test).

strated that MVM-induced NE disruptions can be detected in mouse fibroblast cells infected with MVM as distinct gaps in the nuclear rim immunofluorescence (IF) staining of the nuclear lamins (6). Having found that caspases were implicated in MVM-induced NE disruption in semipermeabilized cells and microinjected *Xenopus* oocytes, we set out to examine the effect of caspase inhibitors on nuclear lamin immunostaining in MVM-infected mouse fibroblast cells using IF microscopy. While mock-infected cells displayed continuous nuclear rim

immunostaining of lamin A/C, abnormal gaps were observed in the lamin A/C immunostaining of MVM-infected cells at 2 h postinfection (Fig. 4A). These gaps coincided with the location of the virus in the cell. In addition, a "cloud" of lamin immunostaining was observed around these nuclear rim gaps. However, when cells were infected with MVM in the presence of the pancaspase inhibitor zVAD-fmk, gaps in the lamin A/C immunostaining were no longer observed (Fig. 4A). Moreover, like zVAD-fmk, the caspase-3 inhibitor zDEVD-fmk also pre-
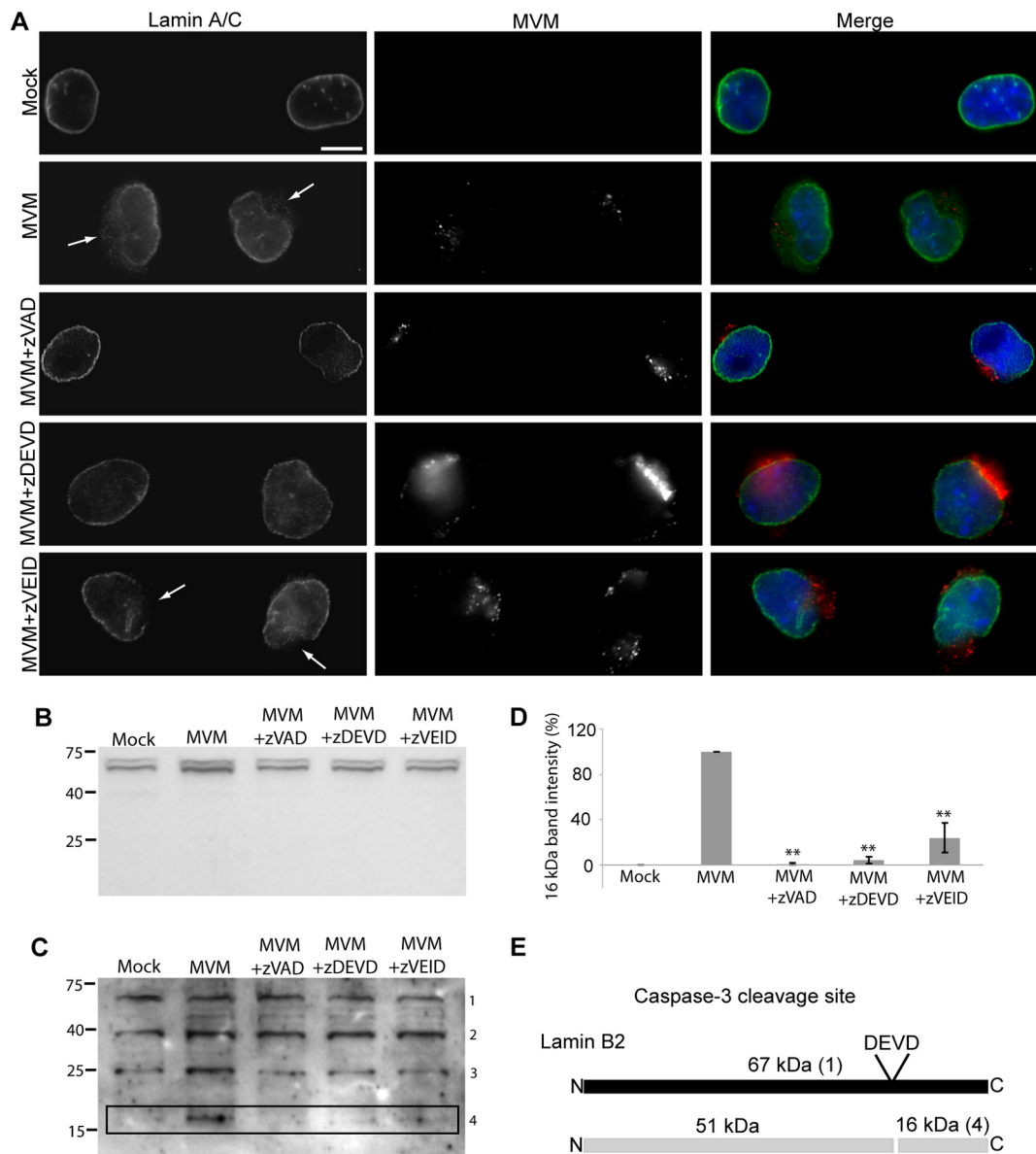
FIG. 4. Caspase inhibitors prevent nuclear lamina disruption and lamin cleavage in MVM-infected cells. (A) LA9 cells were mock infected or infected with MVM (MOI of 4) for 2 h in the presence or absence of a 200 μM concentration of the pancaspase inhibitor zVAD-fmk, the caspase-3 inhibitor zDEVD-fmk, or the caspase-6 inhibitor zVEID-fmk. Cells were immunolabeled with antibodies against lamin A/C (green) and MVM (red). DNA was detected with DAPI (blue). While mock-infected cells showed continuous nuclear rim staining of the lamin A/C, gaps were seen in the lamin A/C immunostaining of MVM-infected cells (indicated by arrows). zVAD-fmk and zDEVD-fmk completely inhibited the MVM-induced nuclear lamina disruption, but zVEID-fmk did not. Scale bar, 5 μm. (B) Western blot for A/C-type lamins in LA9 cells that were mock infected or infected with MVM (MOI of 4) for 2 h in the presence or absence of a 100 μM concentration of the pancaspase inhibitor zVAD-fmk, the caspase-3 inhibitor zDEVD-fmk, or the caspase-6 inhibitor zVEID-fmk. Molecular weights (in thousands) are indicated on the left. (C) The same blot shown in panel B was probed for B-type lamins. Molecular weights (in thousands) are indicated on the left. Numbers on the right indicate the corresponding protein in panel E. (D) Quantification of the band intensity of the 16-kDa cleavage product shown in panel C. The band intensity was quantified and normalized so that mock was 0 and MVM was 100%. Values are means and standard errors from three films. ∗∗, $P < 0.01$ compared to MVM (unpaired Student t test). (E) Schematic showing a putative caspase-3 (DEVD) cleavage site in lamin B2, as well as the sizes of predicted cleavage products. Numbers in parentheses indicate the corresponding band in panel C.

vented the appearance of gaps in the nuclear lamin immuno-staining of MVM-infected cells, while the caspase-6 inhibitor zVEID-fmk did not (Fig. 4A). These results indicate that caspase-3 is involved in MVM-mediated NE disruption during infection of live cells.

In addition, we observed differences in the localization of

MVM in the presence or absence of caspase inhibitors (Fig. 4A). In infected cells not treated with inhibitor or treated with the caspase-6 inhibitor zVEID-fmk, the virus displayed a fairly dispersed localization at 2 h postinfection. However, in infected cells treated with pancaspase or caspase-3 inhibitor, virus capsids appeared to accumulate in a perinuclear location,

suggesting that inhibition of MVM-induced NE disruption prevented nuclear entry of the virus and perhaps also capsid disassembly.

Since caspases are capable of cleaving lamins and because we observed disruption of the nuclear lamina in MVM-infected cells, we next asked whether nuclear lamins were cleaved in MVM-infected cells. The mammalian nuclear lamina is composed of A/C-type lamins, which are products of alternative splicing, as well as lamin B1 and lamin B2, which are encoded by two additional genes (12). We examined lysates from cells that were mock infected or infected with MVM for 2 h for the presence of lamin cleavage products. Western blotting with an anti-lamin A/C antibody yielded two bands of the predicted molecular weights, but no cleavage products were observed (Fig. 4B), although the antibody recognized a lamin A/C cleavage product in a control sample treated with STS (data not shown).

In contrast, Western blotting with an anti-B-lamin antibody revealed the presence of a 16-kDa cleavage product in lysates from MVM-infected but not mock-infected cells (Fig. 4C, lanes Mock and MVM, band 4). When cells were infected with MVM in the presence of the pancaspase inhibitor zVAD-fmk or the caspase-3 inhibitor zDEVD-fmk, the amount of this 16-kDa cleavage product was dramatically reduced (Fig. 4C, lanes MVM+zVAD and MVM+zDEVD, and D). In cells infected in the presence of the caspase-6 inhibitor zVEID-fmk, the abundance of the 16-kDa cleavage product was also reduced, but not as much as in the zVAD or zDEVD lanes (Fig. 4C, lane MVM+zVEID, and D). These results indicate that the 16-kDa band observed in MVM-infected cells is a caspase-3 cleavage product of either lamin B1 or lamin B2. Examination of the amino acid sequences of lamin B1 and lamin B2 (available in the GenBank database at http://www.ncbi.nlm.nih.gov/GenBank/) suggested the presence of a caspase-3 consensus site (DEVD) at the appropriate location in lamin B2 but not lamin B1 (Fig. 4E). Thus, we propose that the 16-kDa band observed in MVM-infected cells is a caspase-3 cleavage product of lamin B2. The partial inhibition of this cleavage in MVM-infected cells treated with the caspase-6 inhibitor zVEID-fmk is likely due to nonspecific effects of the inhibitor. In addition to the 16-kDa band observed in some of the lanes, three additional bands with molecular masses of 67 kDa, 41 kDa, and 26 kDa were present in every lane (Fig. 4C, bands 1 to 3). The 67-kDa band corresponds to full-length lamin B1 and lamin B2, while bands 2 and 3 are likely nonspecific. The fact that we do not observe the predicted 51-kDa cleavage product (Fig. 4E) is likely because the antibody used was raised against a peptide mapping to the lamin B C terminus. Our results suggest that during infection of cells with MVM, lamin B2 is cleaved by caspase-3. This results in a change in the organization of A/C-type lamins, even though they themselves are not cleaved. The altered organization of A/C-type lamins is detectable by IF microscopy, as seen in Fig. 4A.

MVM-induced NE disruption is transient and does not coincide with complete apoptosis. The involvement of caspases in MVM-induced lamin cleavage and NE disruption suggests that at least part of the cellular apoptosis machinery is being used. However, previous work has not found any indication of apoptosis in parvovirus-infected cells until about 72 h postinfection, after viral replication has occurred (28, 35, 41, 43). We there-
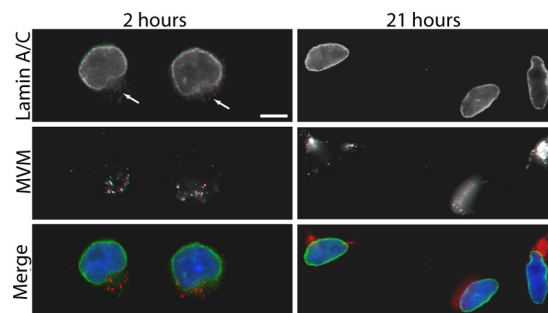

FIG. 5. Nuclear lamina disruption in MVM-infected cells is a transient event. LA9 cells were infected with MVM at an MOI of 4 and prepared for indirect IF at 2 or 21 h after infection. Cells were immunolabeled with antibodies against lamin A/C (green) and MVM (red). DNA was detected with DAPI (blue). Unlike at 2 h postinfection, no nuclear rim gaps are seen in the lamin A/C immunostaining at 21 h postinfection. Gaps in lamin A/C immunostaining are indicated by arrows. Scale bar, 5 μm.

fore examined whether our infection protocol was causing premature apoptosis of MVM-infected cells. Mouse fibroblast cells were infected and stained for double-strand DNA breaks using a terminal deoxynucleotidyltransferase-mediated dUTP-biotin nick end labeling (TUNEL) assay at various times postinfection. We did not observe TUNEL staining in infected cells until 48 h after infection, at which time a small proportion of the cells started to stain positive for double-strand DNA breaks (data not shown).

In addition, we examined the nuclear lamina by IF microscopy at later time points during infection. Unlike at 2 h postinfection, at 21 h postinfection no nuclear rim gaps could be seen in the lamin A/C immunostaining of MVM-infected cells (Fig. 5), suggesting that the nuclear lamina is repaired later during infection. Together these results indicate that the MVM-induced NE disruptions that we observe at 2 h after infection are a local, transient event. These disruptions do not coincide with complete apoptosis, which occurs beginning 48 h after infection at a time when viral replication has already occurred.

Caspase-3 is not activated above basal levels in MVM-infected cells but is relocalized. Based on our results implicating caspase-3 in MVM-induced NE disruption, we next examined whether caspase-3 was activated in MVM-infected cells. A colorimetric caspase-3 activity assay revealed that there was no difference in the amounts of active caspase-3 in lysates from mock-infected and MVM-infected cells at 2 h postinfection, although lysates from cells induced to undergo apoptosis by treatment with STS had robust caspase-3 activity (Fig. 6A). Although caspase-3 was not activated above basal levels in MVM-infected cells, both mock- and MVM-infected cells did exhibit some caspase-3 activity (Fig. 6A). Caspase-3 exists as a proenzyme which must be proteolytically cleaved to become activated. Though caspase-3 is cleaved and activated primarily during apoptosis, low levels of active caspase-3 may exist at a basal state. When we visualized cleaved (activated) caspase-3 in mock- and MVM-infected cells by confocal IF microscopy at 2 h postinfection, we noticed a change in the localization of cleaved caspase-3 in MVM-infected cells. While cleaved caspase-3 was completely excluded from the nucleus in mock-infected cells, in MVM-infected cells some of the cleaved
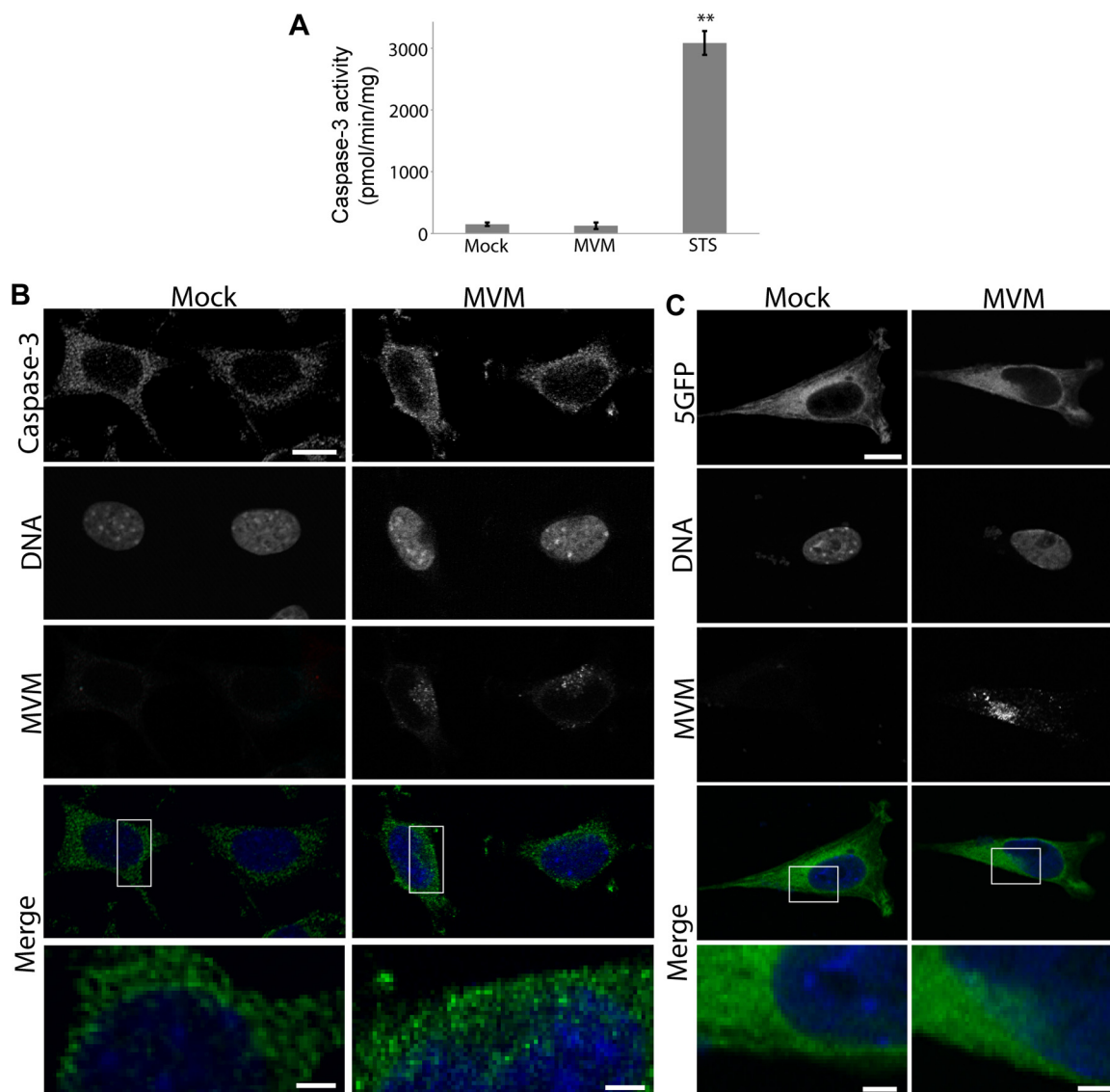
FIG. 6. Cleaved caspase-3 and a fluorescent cytoplasmic reporter are mislocalized in MVM-infected cells. (A) Colorimetric assay for caspase-3 activity in lysates from mock-infected, MVM-infected (MOI of 4, 2-h infection), and STS-treated cells. Values are means and standard errors measured for three independent experiments. ∗∗, $P < 0.01$ compared to mock infection (unpaired Student t test). (B) LA9 cells were mock infected or infected with MVM at an MOI of 4 and prepared for indirect IF at 2 h after infection. Cells were immunolabeled with antibodies against cleaved caspase-3 (green) and MVM (red), while DNA was detected with DAPI (blue). The merge shows green and blue only; the bottom panels represent higher-magnification images of the areas indicated in white boxes above. Cleaved caspase-3 was excluded from the nucleus in mock-infected cells but entered the nucleus in MVM-infected cells. Scale bar, 5 μm (inset, 1 μm). (C) LA9 cells transiently expressing 5GFP (green) were mock infected or infected with MVM at an MOI of 4 and prepared for indirect IF at 2 h after infection. Cells were immunolabeled with antibodies against MVM (red), and DNA was detected with DAPI (blue). The merge shows green and blue only; the bottom panels represent higher-magnification images of the areas indicated in white boxes above. The 5GFP was excluded from the nucleus in mock-infected cells but entered the nucleus in MVM-infected cells. Scale bar, 5 μm (inset, 1 μm).

caspase-3 appeared to leak into the nucleus, in close proximity to the location of the virus in the cell (Fig. 6B). This suggests that previously cleaved, activated caspase-3 already present at low levels in the cytoplasm gains access to the nucleus because of MVM-induced nuclear membrane disruption; once inside the nucleus, caspase-3 likely plays a role in lamin cleavage and progression of NE disruption.

Cytoplasmic proteins other than active caspase-3 are also relocalized in MVM-infected cells. To examine whether the relocalization of cleaved caspase-3 in MVM-infected cells was

a specific effect, we also looked at the localization of another cytoplasmic protein. We transiently transfected cells with a construct encoding five green fluorescent protein molecules in tandem (5GFP) (construct courtesy of G. Lukacs, McGill University) and examined the localization of the 5GFP in mock-infected and MVM-infected cells by confocal microscopy at 2 h postinfection. We chose 5GFP because this is the smallest number of tandem GFP molecules that is completely excluded from the nucleus under normal conditions (59). Similarly to cleaved caspase-3, 5GFP was completely excluded from the
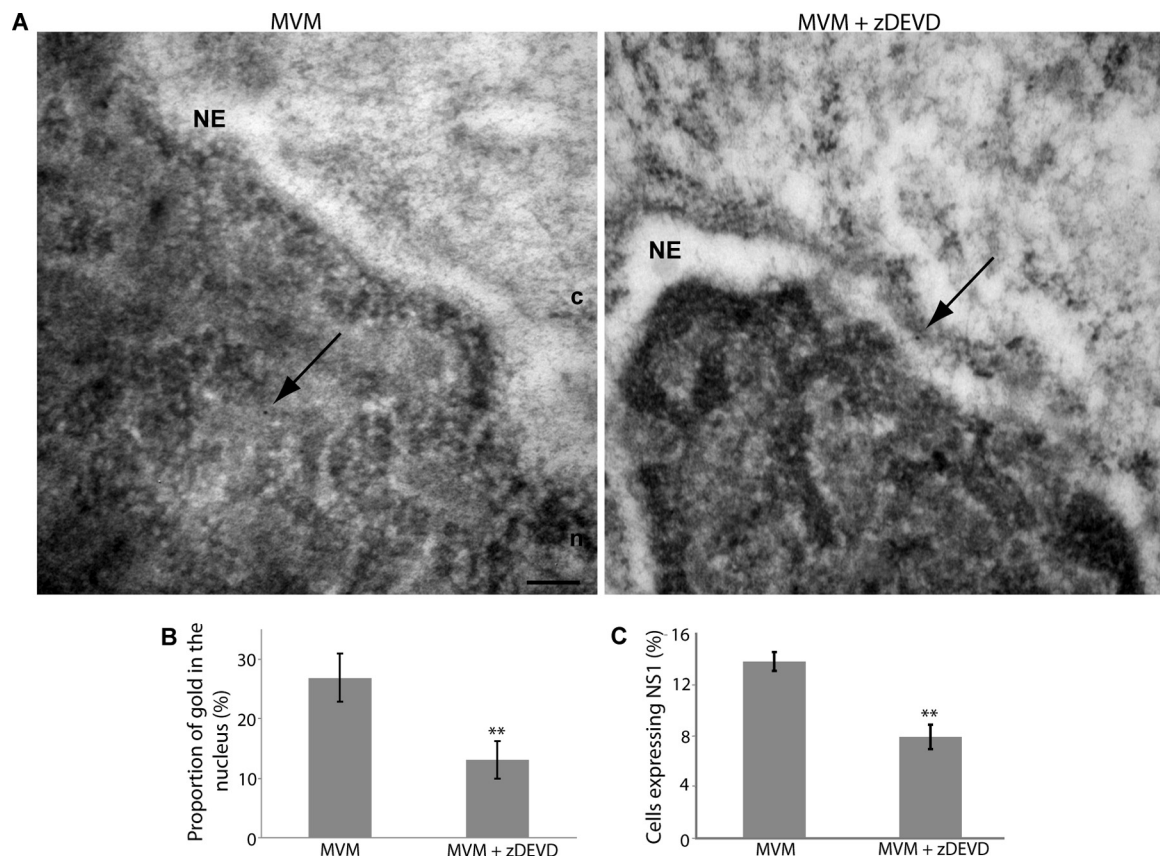
FIG. 7. NE disruption facilitates nuclear entry of MVM capsids and viral gene expression. (A) LA9 cells were infected with MVM (MOI of 4) for 2 h in the presence or absence of a 100 μM concentration of the caspase-3 inhibitor zDEVD-fmk. Cells were then prepared for thin-section EM and immunolabeled with anticapsid antibody and 10-nm-gold-conjugated secondary antibody (indicated by arrows). In cells infected with MVM in the absence of zDEVD-fmk, gold particles were frequently observed in the nucleus. In cells infected with MVM in the presence of zDEVD-fmk, gold particles were less frequently observed in the nucleus; instead, gold particles were often observed at the cytoplasmic side of the NE. c, cytoplasm; n, nucleus; NE, nuclear envelope. Scale bar, 200 nm. (B) Mean proportion of gold in the nucleus and standard error for 60 cells per condition, from two independent experiments performed as described above. ∗∗, $P < 0.01$ compared to MVM (unpaired Student t test). (C) LA9 cells were infected with MVM (MOI of 4) for 15 h in the presence or absence of a 200 μM concentration of the caspase-3 inhibitor zDEVD-fmk. Cells were immunolabeled with an antibody against NS1, and DNA was detected with DAPI. The proportion of cells expressing NS1 was quantified using threshold analysis. Values are means and standard errors measured from four independent experiments; approximately 2,000 cells were counted for each condition for each experiment. ∗∗, $P < 0.01$ compared to mock (unpaired Student t test).

nucleus in mock-infected cells; however, in MVM-infected cells some of the 5GFP leaked into the nucleus, again in close proximity to the location of the virus in the cell (Fig. 6C). Thus, infection with MVM seems to alter the compartmentalization of multiple host proteins.

NE disruption facilitates entry of MVM capsids into the nucleus and is important for the MVM replication cycle. To investigate whether NE disruption can facilitate nuclear entry of MVM during infection, we next analyzed the effect of caspase-3 inhibition on the subcellular localization of MVM capsids using immunogold EM. Mock-infected cells and cells infected with MVM for 2 h in the absence or presence of zDEVD-fmk were subjected to immunogold EM using an anti-MVM monoclonal antibody, which recognizes intact capsids. As expected, immunogold labeling was very rarely observed in mock-infected cells. In contrast, gold particles, indicating the location of intact MVM capsids, were observed in multiple locations throughout infected cells. Quantification of the label indicated that at 2 h postinfection nearly 30% of the gold

observed in thin sections through the nuclei of MVM-infected cells was located inside the nucleus (Fig. 7A and B), suggesting that the timing of NE disruption is consistent with the timing of nuclear entry of a significant number of MVM capsids. Strikingly, in cells infected with MVM in the presence of zDEVD-fmk, gold particles were more often observed at the cytoplasmic side of the NE (Fig. 7A), and only 13% of the gold observed was located in the nucleus (Fig. 7B). This strongly suggests that caspase-3-facilitated NE disruptions can mediate entry of intact MVM capsids into the nuclei of infected cells. Unfortunately, the NE ultrastructure could not be carefully examined in immunogold-labeled samples, since the osmium tetroxide fixation step necessary to clearly visualize membranes was not included in the preparation of the samples because it destroys the antigenicity of proteins.

Lastly, we investigated whether the reduced nuclear entry of MVM under conditions of caspase-3 inhibition affected later stages of the replication cycle of MVM. To do this we examined the effect of the caspase-3 inhibitor zDEVD-fmk on ex-

pression of the viral nonstructural protein 1 (NS1). NS1 is not present on the MVM capsid in large amounts (9). Therefore, the presence of NS1 in MVM-infected cells indicates that the viral genome has successfully entered the nucleus of the host cell and that expression of viral proteins has begun. When cells were infected with MVM at an MOI of 4 for 15 h followed by visualization of NS1 by IF microscopy, NS1 could be detected in approximately 15% of the infected cells; however, when cells were infected in the presence of zDEVD-fmk, the proportion of cells detectably expressing NS1 decreased by half (Fig. 7C). This indicates that caspase-mediated NE disruption plays an important role in the MVM replication cycle.

DISCUSSION

Mechanism of MVM-induced NE disruption. Previously we found that the parvovirus MVM causes small disruptions in the NE and nuclear lamina of infected fibroblast cells as early as 1 h postinfection (6). We have now investigated the molecular mechanism by which MVM induces NE disruption. Four separate assays, i.e., a semipermeabilized cell assay for NE permeability, EM visualization of the NE of microinjected *Xenopus* oocytes, lamin immunostaining, and Western blotting of lamins in MVM-infected cells, all support a role for cellular caspase-3 activity in MVM-mediated disruption of the NE. Western blotting results suggest that lamin B2 is cleaved at a caspase-3 consensus site in MVM-infected cells (Fig. 4). Consistent with our results, it has been shown that during apoptosis, lamin A is cleaved by caspase-6, while a B lamin is cleaved by caspase-3 (50). Thus, we have focused primarily on the role of caspase-3 in this process. Although we observed caspase-mediated disruption of the nuclear lamina in MVM-infected cells early during infection, apoptosis leading to double-strand DNA breaks did not occur until 48 h postinfection. While caspases are usually described as apoptotic proteases, a variety of nonapoptotic functions have also been discovered for these enzymes (17); for example, caspase-3 is upregulated and activated just prior to mitosis, suggesting that it may play a role in the G_2/M transition (27). Here we propose a nonapoptotic role for caspase-3 in the parvovirus replication cycle.

Caspase-3 was not activated above basal levels in MVM-infected cells. However, previously cleaved caspase-3 present at low levels under basal conditions showed relocalization to the nucleus in infected cells (Fig. 6). Based on these observations, we propose a model in which MVM induces disruption of the nuclear membranes by an as-yet-unknown mechanism, not involving viral PLA2 activity; this membrane disruption allows previously cleaved and activated caspase-3 in the cytoplasm to gain access to the nucleus, where the protease cleaves lamin B2, resulting in disruption of the nuclear lamina structure and progression of NE disruptions (Fig. 8). In the absence of lamina perturbation, it is probable that the initial membrane disruptions reseal very quickly, which is likely why we do not observe membrane disruption in oocytes coinjected with MVM and a pancaspase or caspase-3 inhibitor (Fig. 3). The fact that a B-type lamin was cleaved in MVM-infected cells while A/C-type lamins were not is consistent with a recently proposed model of the nuclear lamina in which the regular structure directly underlying the NE is composed of B-type lamins, while A/C-type lamins form sparser bundles which lie beneath (20);
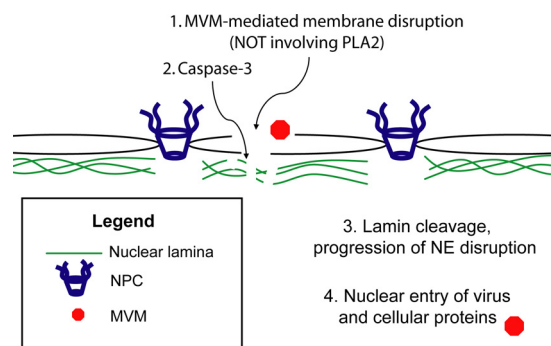

FIG. 8. Model of MVM-induced NE disruption. MVM induces disruption of the nuclear membranes by a mechanism that does not involve viral PLA2 activity (1). Previously cleaved, activated caspases in the cytoplasm gain access to the nucleus (2), where they cleave B-type lamins (3). This cleavage is necessary for sustained disruption of the NE, which in turn mediates nuclear entry of the MVM capsid and possibly other cellular proteins required by the virus for replication (4).

thus, caspases gaining access to the nuclear lamina from the cytoplasmic side would encounter primarily B-type lamins rather than A/C-type lamins. Our observations that inhibition of caspase-3 in MVM-infected cells reduced nuclear entry of MVM capsids and expression of NS1 (Fig. 7) suggest that caspase-facilitated NE disruption plays a role in delivery of the MVM genome into the nucleus of the host cell. The virus-induced NE disruption also alters the compartmentalization of cellular proteins other than cleaved caspase-3, as demonstrated here for exogenous 5GFP (Fig. 6). It is possible that relocalization of certain cytoplasmic proteins to the nucleus is beneficial for viral replication or assembly.

Nuclear entry of parvoviruses. Several lines of evidence point to NE disruption as the mechanism of parvoviral entry into the nucleus. When MVM is microinjected into *Xenopus* oocytes and visualized by EM, virions are observed in close proximity to disruptions of the ONM and in the intermembrane space between the INM and ONM (7). In addition, in *Xenopus* oocytes preinjected with the lectin wheat germ agglutinin (WGA) to block transport through the NPC, microinjection of MVM causes NE disruptions which support nuclear entry of proteins in an NPC-independent manner (7). Consistent with these data, blocking NPCs with WGA does not prevent uptake of AAV2 into purified nuclei (24). Lastly, the number of MVM capsids entering the nucleus in infected cells was reduced when NE disruption was inhibited with the caspase-3 inhibitor zDEVD-fmk (Fig. 7).

The nature of the parvoviral infectious entity penetrating the nucleus has been somewhat controversial. There is evidence that the parvoviral genome enters the nucleus in association with an intact capsid. Multiple studies using IF microscopy or GFP- or fluorophore-conjugated virions have detected parvoviral capsid proteins in the nuclei of infected cells (3, 33, 34, 48, 58). In addition, microinjection of antibodies against the capsid of AAV2 into the nucleus can inhibit productive infection of tissue culture cells (52). Lastly, immunogold EM has revealed intact capsids of canine parvovirus in the nuclei of cells infected in the presence of cycloheximide, which prevents the synthesis of new capsid proteins (53). In contrast, several stud-

ies have noted that only very small amounts of capsid protein are detected in the nucleus, causing the authors to suggest that the genome dissociates from the capsid prior to nuclear entry (33, 34). Our immunogold EM results support the notion that the MVM genome enters the host nucleus in association with an intact capsid.

The parvoviral nuclear entry mechanism through disruptions of the NE is unlike that of any other virus known to date. The majority of viruses use nuclear localization signals (NLSs) in viral proteins to bind soluble cellular transport receptors, which then mediate nuclear import of the viral genome through the NPC (21, 26, 60, 61). Like for other viruses, it has been shown that parvoviruses have functional NLSs in their capsid proteins (32, 57). It has been demonstrated that these NLSs are necessary for nuclear import of capsid protein trimers prior to virion assembly in the nucleus (44) and that nuclear import of capsid protein trimers is dependent on phosphorylation by Raf-1 (45). One of the parvovirus NLSs, within VP2, is buried inside the capsid of assembled virions and could not be involved in nuclear entry of the incoming capsid during initial infection (1, 31). The others, within VP1, are initially buried within the capsid as well; these NLSs are located within a region of VP1 which becomes exposed during endocytic trafficking of the capsid (8, 34), and they could potentially participate in transport of the capsid through the NPC. However, it has not been demonstrated that these NLSs become sufficiently exposed to be able to interact with cellular import receptors in order to mediate nuclear import of the capsid. If the VP1 NLSs do become sufficiently exposed to interact with importins, then it is possible that they play a role in targeting the MVM capsid to the NE prior to nuclear entry via NE disruptions. In addition, it has recently been shown that an NLS-like sequence in the VP1 of AAV2 plays a role in targeting capsids to the nucleolus (29). Thus, it is possible that the VP1 NLSs function primarily in intranuclear trafficking rather than in trafficking of parvovirus capsids to the nucleus.

Other viruses that disrupt the NE. One virus that may use a nuclear import strategy similar to that of parvoviruses is human immunodeficiency virus (HIV). The HIV viral protein R (Vpr) can induce transient disruptions of the NE (13), and it has been proposed that these disruptions may mediate nuclear import of the HIV preintegration complex (47). However, it is thought that Vpr enters the nucleus and induces disruptions from the nuclear rather than the cytoplasmic side of the NE (47), distinguishing the proposed HIV nuclear entry mechanism from the one used by parvoviruses. Other viruses also alter the NE during infection, although they do so for different reasons. For example, cytomegalovirus and herpes simplex virus type 1 both disrupt the nuclear lamina to facilitate viral egress from the nucleus (37, 49). Interestingly, the partial relocalization of 5GFP from the cytoplasm to the nucleus that we observed in MVM-infected cells is very similar to that seen when cells infected with human cytomegalovirus are loaded with large fluorescent dextran and then visualized at 72 h postinfection (4). The restricted localization of cytoplasmic markers to a small region of the nucleus in both cases suggests that there are structures in the nucleus which prevent rapid diffusion of these molecules. Perhaps incomplete disruption of the nuclear lamina causes proteins or dextrans to become trapped between the NE and the partially dissolved lamin

meshwork. In contrast, several cytoplasmically replicating RNA viruses target NPC proteins for degradation, likely in order to interfere with the host interferon response (22). Thus, alteration to the NE and associated structures in virus-infected cells is a common theme; however, disruption of the NE to gain access to the nucleus is rare. We are unaware of any other examples of viruses making use of host apoptotic machinery during trafficking of incoming virions prior to virus gene expression and replication. Our findings represent a novel mechanism by which a virus uses host enzymes to gain access to the nucleus during infection.

REFERENCES

1. **Agbandje-McKenna, M., A. L. Llamas-Saiz, F. Wang, P. Tattersall, and M. G. Rossmann.** 1998. Functional implications of the structure of the murine parvovirus, minute virus of mice. Structure **6:**1369–1381.
2. **Au, S., S. Cohen, and N. Panté.** 2010. Microinjection of Xenopus laevis oocytes as a system for studying nuclear transport of viruses. Methods **51:**114–120.
3. **Bartlett, J. S., R. Wilcher, and R. J. Samulski.** 2000. Infectious entry pathway of adeno-associated virus and adeno-associated virus vectors. J. Virol. **74:**2777–2785.
4. **Buchkovich, N. J., T. G. Maguire, and J. C. Alwine.** 2010. Role of the endoplasmic reticulum chaperone BiP, SUN domain proteins, and dynein in altering nuclear morphology during human cytomegalovirus infection. J. Virol. **84:**7005–7017.
5. **Cohen, S., S. Au, and N. Panté.** 2009. Microinjection of Xenopus laevis oocytes. J. Vis. Exp. **24:**1106. doi:10.3791/1106.
6. **Cohen, S., A. R. Behzad, J. B. Carroll, and N. Panté.** 2006. Parvoviral nuclear import: bypassing the host nuclear-transport machinery. J. Gen. Virol. **87:**3209–3213.
7. **Cohen, S., and N. Panté.** 2005. Pushing the envelope: microinjection of minute virus of mice into Xenopus oocytes causes damage to the nuclear envelope. J. Gen. Virol. **86:**3243–3252.
8. **Cotmore, S. F., M. A. D'Abramo, Jr, C. M. Ticknor, and P. Tattersall.** 1999. Controlled conformational transitions in the MVM virion expose the VP1 N-terminus and viral genome without particle disassembly. Virology **254:**169–181.
9. **Cotmore, S. F., and P. Tattersall.** 1989. A genome-linked copy of the NS-1 polypeptide is located on the outside of infectious parvovirus particles. J. Virol. **63:**3902–3911.
10. **Cotmore, S. F., and P. Tattersall.** 2007. Parvoviral host range and cell entry mechanisms. Adv. Virus Res. **70:**183–232.
11. **Cros, J. F., and P. Palese.** 2003. Trafficking of viral genomic RNA into and out of the nucleus: influenza, Thogoto and Borna disease viruses. Virus Res. **95:**3–12.
12. **Dechat, T., et al.** 2008. Nuclear lamins: major factors in the structural organization and function of the nucleus and chromatin. Genes Dev. **22:**832–853.
13. **de Noronha, C. M., et al.** 2001. Dynamic disruptions in nuclear envelope architecture and integrity induced by HIV-1 Vpr. Science **294:**1105–1108.
14. **Ekert, P. G., J. Silke, and D. L. Vaux.** 1999. Caspase inhibitors. Cell Death Differ. **6:**1081–1086.
15. **Fahrenkrog, B.** 2006. The nuclear pore complex, nuclear transport, and apoptosis. Can. J. Physiol. Pharmacol. **84:**279–286.
16. **Farr, G. A., L. G. Zhang, and P. Tattersall.** 2005. Parvoviral virions deploy a capsid-tethered lipolytic enzyme to breach the endosomal membrane during cell entry. Proc. Natl. Acad. Sci. U. S. A. **102:**17148–17153.
17. **Feinstein-Rotkopf, Y., and E. Arama.** 2009. Can't live without them, can live with them: roles of caspases during vital cellular processes. Apoptosis **14:**980–995.
18. **Fricker, M., M. Hollinshead, N. White, and D. Vaux.** 1997. Interphase nuclei of many mammalian cell types contain deep, dynamic, tubular membrane-bound invaginations of the nuclear envelope. J. Cell Biol. **136:**531–544.
19. **Goff, S. P.** 2007. Host factors exploited by retroviruses. Nat. Rev. Microbiol. **5:**253–263.

20. **Goldberg, M. W., J. Fiserova, I. Huttenlauch, and R. Stick.** 2008. A new model for nuclear lamina organization. Biochem. Soc. Trans. **36:**1339–1343.
21. **Greber, U. F., and M. Fornerod.** 2005. Nuclear import in viral infections. Curr. Top. Microbiol. Immunol. **285:**109–138.
22. **Gustin, K. E.** 2003. Inhibition of nucleo-cytoplasmic trafficking by RNA viruses: targeting the nuclear pore complex. Virus Res. **95:**35–44.
23. **Guttinger, S., E. Laurell, and U. Kutay.** 2009. Orchestrating nuclear envelope disassembly and reassembly during mitosis. Nat. Rev. Mol. Cell Biol. **10:**178–191.
24. **Hansen, J., K. Qing, and A. Srivastava.** 2001. Infection of purified nuclei by adeno-associated virus 2. Mol. Ther. **4:**289–296.
25. **Harbison, C. E., J. A. Chiorini, and C. R. Parrish.** 2008. The parvovirus capsid odyssey: from the cell surface to the nucleus. Trends Microbiol. **16:**208–214.
26. **Helenius, A.** 2007. Virus entry and uncoating, p. 99–118. *In* D. M. Knipe (ed.), Fields virology, vol. 1. Lippincott Williams & Wilkins, Philadelphia, PA.
27. **Hsu, S. L., et al.** 2006. Caspase 3, periodically expressed and activated at G2/M transition, is required for nocodazole-induced mitotic checkpoint. Apoptosis **11:**765–771.
28. **Ikeda, Y., et al.** 1998. Apoptosis in feline panleukopenia virus-infected lymphocytes. J. Virol. **72:**6932–6936.
29. **Johnson, J. S., et al.** 2010. Mutagenesis of adeno-associated virus type 2 capsid protein VP1 uncovers new roles for basic amino acids in trafficking and cell-specific transduction. J. Virol. **84:**8888–8902.
30. **Littlefield, J. W.** 1964. The selection of hybrid mouse fibroblasts. Cold Spring Harbor Symp. Quant. Biol. **29:**161–166.
31. **Lombardo, E., J. C. Ramirez, M. Agbandje-McKenna, and J. M. Almendral.** 2000. A beta-stranded motif drives capsid protein oligomers of the parvovirus minute virus of mice into the nucleus for viral assembly. J. Virol. **74:**3804–3814.
32. **Lombardo, E., J. C. Ramirez, J. Garcia, and J. M. Almendral.** 2002. Complementary roles of multiple nuclear targeting signals in the capsid proteins of the parvovirus minute virus of mice during assembly and onset of infection. J. Virol. **76:**7049–7059.
33. **Lux, K., et al.** 2005. Green fluorescent protein-tagged adeno-associated virus particles allow the study of cytosolic and nuclear trafficking. J. Virol. **79:**11776–11787.
34. **Mani, B., et al.** 2006. Low pH-dependent endosomal processing of the incoming parvovirus minute virus of mice virion leads to externalization of the VP1 N-terminal sequence (N-VP1), N-VP2 cleavage, and uncoating of the full-length genome. J. Virol. **80:**1015–1024.
35. **Morey, A. L., D. J. Ferguson, and K. A. Fleming.** 1993. Ultrastructural features of fetal erythroid precursors infected with parvovirus B19 in vitro: evidence of cell death by apoptosis. J. Pathol. **169:**213–220.
36. **Muhlhausser, P., and U. Kutay.** 2007. An in vitro nuclear disassembly system reveals a role for the RanGTPase system and microtubule-dependent steps in nuclear envelope breakdown. J. Cell Biol. **178:**595–610.
37. **Muranyi, W., J. Haas, M. Wagner, G. Krohne, and U. H. Koszinowski.** 2002. Cytomegalovirus recruitment of cellular kinases to dissolve the nuclear lamina. Science **297:**854–857.
38. **Orth, K., A. M. Chinnaiyan, M. Garg, C. J. Froelich, and V. M. Dixit.** 1996. The CED-3/ICE-like protease Mch2 is activated during apoptosis and cleaves the death substrate lamin A. J. Biol. Chem. **271:**16443–16446.
39. **Panté, N.** 2006. Use of intact Xenopus oocytes in nucleocytoplasmic transport studies. Methods Mol. Biol. **322:**301–314.
40. **Panté, N., and M. Kann.** 2002. Nuclear pore complex is able to transport macromolecules with diameters of about 39 nm. Mol. Biol. Cell **13:**425–434.
41. **Poole, B. D., Y. V. Karetnyi, and S. J. Naides.** 2004. Parvovirus B19-induced apoptosis of hepatocytes. J. Virol. **78:**7775–7783.
42. **Rabe, B., A. Vlachou, N. Panté, A. Helenius, and M. Kann.** 2003. Nuclear import of hepatitis B virus capsids and release of the viral genome. Proc. Natl. Acad. Sci. U. S. A. **100:**9849–9854.
43. **Rayet, B., J. A. Lopez-Guerrero, J. Rommelaere, and C. Dinsart.** 1998. Induction of programmed cell death by parvovirus H-1 in U937 cells: connection with the tumor necrosis factor alpha signalling pathway. J. Virol. **72:**8893–8903.
44. **Riolobos, L., J. Reguera, M. G. Mateu, and J. M. Almendral.** 2006. Nuclear transport of trimeric assembly intermediates exerts a morphogenetic control on the icosahedral parvovirus capsid. J. Mol. Biol. **357:**1026–1038.
45. **Riolobos, L., et al.** 2010. Viral oncolysis that targets Raf-1 signaling control of nuclear transport. J. Virol. **84:**2090–2099.
46. **Robertson, J. D., S. Orrenius, and B. Zhivotovsky.** 2000. Nuclear events in apoptosis. J. Struct. Biol. **129:**346–358.
47. **Segura-Totten, M., and K. L. Wilson.** 2001. Virology HIV—breaking the rules for nuclear entry. Science **294:**1016–1017.
48. **Seisenberger, G., et al.** 2001. Real-time single-molecule imaging of the infection pathway of an adeno-associated virus. Science **294:**1929–1932.
49. **Simpson-Holley, M., R. C. Colgrove, G. Nalepa, J. W. Harper, and D. M. Knipe.** 2005. Identification and functional evaluation of cellular and viral factors involved in the alteration of nuclear architecture during herpes simplex virus 1 infection. J. Virol. **79:**12840–12851.
50. **Slee, E. A., C. Adrain, and S. J. Martin.** 2001. Executioner caspase-3, -6, and -7 perform distinct, non-redundant roles during the demolition phase of apoptosis. J. Biol. Chem. **276:**7320–7326.
51. **Sodeik, B., M. W. Ebersold, and A. Helenius.** 1997. Microtubule-mediated transport of incoming herpes simplex virus 1 capsids to the nucleus. J. Cell Biol. **136:**1007–1021.
52. **Sonntag, F., S. Bleker, B. Leuchs, R. Fischer, and J. A. Kleinschmidt.** 2006. Adeno-associated virus type 2 capsids with externalized VP1/VP2 trafficking domains are generated prior to passage through the cytoplasm and are maintained until uncoating occurs in the nucleus. J. Virol. **80:**11040–11054.
53. **Suikkanen, S., et al.** 2003. Exploitation of microtubule cytoskeleton and dynein during parvoviral traffic toward the nucleus. J. Virol. **77:**10270–10279.
54. **Takahashi, A., et al.** 1996. CrmA/SPI-2 inhibition of an endogenous ICE-related protease responsible for lamin A cleavage and apoptotic nuclear fragmentation. J. Biol. Chem. **271:**32487–32490.
55. **Terry, L. J., E. B. Shows, and S. R. Wente.** 2007. Crossing the nuclear envelope: hierarchical regulation of nucleocytoplasmic transport. Science **318:**1412–1416.
56. **Thornberry, N. A., et al.** 1997. A combinatorial approach defines specificities of members of the caspase family and granzyme B. Functional relationships established for key mediators of apoptosis. J. Biol. Chem. **272:**17907–17911.
57. **Vihinen-Ranta, M., L. Kakkola, A. Kalela, P. Vilja, and M. Vuento.** 1997. Characterization of a nuclear localization signal of canine parvovirus capsid proteins. Eur. J. Biochem. **250:**389–394.
58. **Vihinen-Ranta, M., et al.** 1998. Intracellular route of canine parvovirus entry. J. Virol. **72:**802–806.
59. **Wang, R., and M. G. Brattain.** 2007. The maximal size of protein to diffuse through the nuclear pore is larger than 60kDa. FEBS Lett. **581:**3164–3170.
60. **Whittaker, G. R.** 2003. Virus nuclear import. Adv. Drug Deliv. Rev. **55:**733–747.
61. **Whittaker, G. R., M. Kann, and A. Helenius.** 2000. Viral entry into the nucleus. Annu. Rev. Cell Dev. Biol. **16:**627–651.